Commensurate antiferromagnetic ordering in Ba(Fe$_{1-x}$Co$_x$)$_2$As$_2$ determined by x-ray resonant magnetic scattering at the Fe K edge

M. G. Kim,[1] A. Kreyssig,[1] Y. B. Lee,[1] J. W. Kim,[2] D. K. Pratt,[1] A. Thaler,[1] S. L. Bud'ko,[1] P. C. Canfield,[1] B. N. Harmon,[1] R. J. McQueeney,[1] and A. I. Goldman[1]

[1]*Ames Laboratory, U.S. DOE and Department of Physics and Astronomy, Iowa State University, Ames, Iowa 50011, USA*
[2]*Advanced Photon Source, Argonne National Laboratory, Argonne, Illinois 60439, USA*
(Received 3 October 2010; published 24 November 2010)

We describe x-ray resonant magnetic diffraction measurements at the Fe K edge of both the parent BaFe$_2$As$_2$ and superconducting Ba(Fe$_{0.953}$Co$_{0.047}$)$_2$As$_2$ compounds. From these high-resolution measurements we conclude that the magnetic structure is commensurate for both compositions. The energy spectrum of the resonant scattering is in reasonable agreement with theoretical calculations using the full-potential linear augmented plane-wave method with a local density functional.

The observation of coexistence and competition between superconductivity (SC) and antiferromagnetic (AFM) order in some members of the iron-arsenide family of superconductors has raised interesting issues regarding the nature of both the SC and AFM states. Several theoretical treatments have demonstrated that coexistence is inconsistent with conventional BCS coupling, whereas the s$^{\pm}$ state, arising from pairing through magnetic fluctuations, is compatible with coexistence and competition between SC and AFM order.[1–5] However, the nature of the AFM state in the doped superconducting compounds, particularly the potential for incommensurability of the magnetic structure, remains a significant issue under debate in both theoretical and experimental work.

It has been argued that an incommensurate magnetic structure is expected for the doped iron arsenides because of imperfect nesting of the hole and electron Fermi surface pockets,[6,7] referencing previous work on chromium.[8] Some theoretical models find that the coexistence between AFM and SC points to incommensurate AFM order.[6,7,9] However, it has also been noted that while incommensurability may broaden the coexistence regime,[10] it does not appear to be a prerequisite for coexistence.[5] Recent calculations[11] of the spin susceptibility in the parent and doped AEFe$_2$As$_2$ (AE = Ca, Ba, Sr) compounds point to incommensurability as the origin of the anisotropy observed in the low-energy spin-fluctuation spectrum of Ba(Fe$_{0.926}$Co$_{0.074}$)$_2$As$_2$.[12]

In contrast to the Fe$_{1+y}$(Te$_{1-x}$Se$_x$) family,[13,14] all neutron-diffraction measurements to date indicate that the AFM order in the doped ROFeAs (R=rare earth) and AEFe$_2$As$_2$ families is commensurate,[4,15–23] and characterized by the so-called "stripelike" magnetic structure.[13,14] Nevertheless, other measurements employing local probes of magnetism, such as ^{75}As nuclear magnetic resonance (NMR),[24] muon spin relaxation (μSR),[25] and ^{57}Fe Mössbauer spectroscopy[26] have proposed that the magnetic order is, in fact, incommensurate for the doped compounds. Zero-field μSR measurements on doped LaFeAs(O$_{0.97}$F$_{0.03}$) noted a much faster damping of the signal than found for the undoped parent compound and attributed this to incommensurate AFM order.[25] Supporting this view, NMR measurements[24,27] on underdoped Ba(Fe$_{1-x}$Co$_x$)$_2$As$_2$ (x=0.02,0.04) (Ref. 27) and (x=0.06) (Ref. 24) found a strong broadening of the ^{75}As lines attrib-

utable to the appearance of a distribution of internal fields at low temperatures in the magnetically ordered state. A quantitative comparison of the line broadening for $\mathbf{H} \| \mathbf{c}$ and $\mathbf{H} \| \mathbf{ab}$ led to the conclusion that there is a small incommensurability, ε, in the magnetic structure such that the commensurate propagation vector $(\frac{1}{2}, \frac{1}{2}, 1)$ in the undoped parent compound is given by $(\frac{1}{2}-\varepsilon, \frac{1}{2}-\varepsilon, 1)$ with ε estimated to be approximately 0.04 reciprocal lattice units (rlu), in the lightly Co-doped compounds.[24]

To resolve this issue we present high-resolution x-ray resonant magnetic scattering (XRMS) measurements at the Fe K edge for two samples: the parent BaFe$_2$As$_2$ compound and Co-doped Ba(Fe$_{0.953}$Co$_{0.047}$)$_2$As$_2$ which manifests coexistence and competition between SC and AFM suggesting the possibility of incommensurate magnetic order. We find that the magnetic Bragg peaks are commensurate for both samples and scans along the $[\zeta \ \zeta \ 0]$ and $[\zeta \ -\zeta \ 0]$ directions allow us to place limits on the magnitude of a potential incommensurability that are much smaller than any value proposed to date. The energy spectrum of the resonant scattering is in reasonable agreement with theoretical calculations using the full-potential linear-augmented plane-wave (FLAPW) method[28] with a local density functional.[29] These calculations suggest that the resonant scattering at the Fe K edge in the σ-to-π scattering channel arises from dipole allowed transitions from the core 1s states to the unoccupied 4p states that are spin polarized due to hybridization with the 3d states close to the Fermi energy.

Single crystals of BaFe$_2$As$_2$ and Ba(Fe$_{0.953}$Co$_{0.047}$)$_2$As$_2$ were grown out of a FeAs self-flux using conventional high-temperature solution growth.[30] Crystals from the same batch have been studied by both neutron[4,22] and x-ray[31] scattering measurements previously. For the XRMS measurements, pieces of the as-grown single crystals of approximate dimensions $3 \times 2 \times 0.03$ mm^3 (BaFe$_2$As$_2$) and $7 \times 4 \times 0.08$ mm^3 [Ba(Fe$_{0.953}$Co$_{0.047}$)$_2$As$_2$] were selected. The extended surfaces of the crystals were perpendicular to the **c** axis. The measured mosaicities of the crystals were less than 0.02° full width at half maximum (FWHM), attesting to the high quality of the samples. The XRMS experiment was performed on the 6ID-B beamline at the Advanced Photon Source at the Fe K edge (E=7.112 keV). The incident radiation was lin-
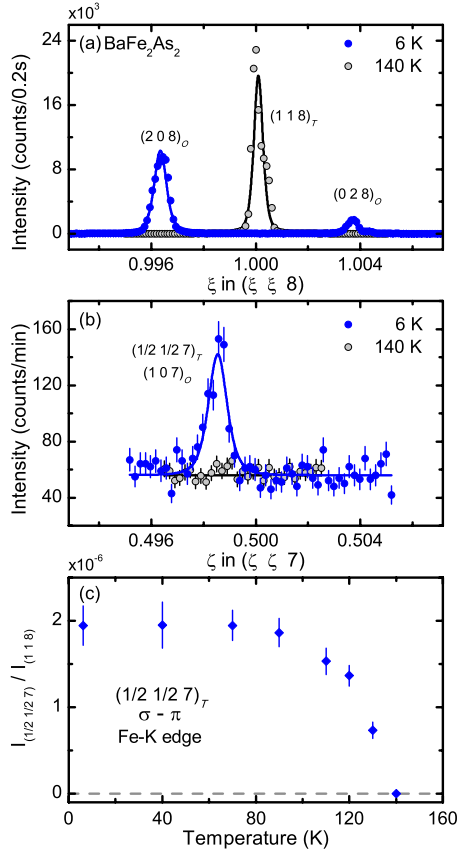
FIG. 1. (Color online) (a) Diffraction data from the parent BaFe$_2$As$_2$ compound characteristic of the tetragonal structure above and the orthorhombic structure below T_S=136 K. (b) Scattering measured in the σ-π channel at the magnetic Bragg peak position of the "stripelike" AFM phase above and below T_N=T_S. (c) The temperature dependence of the integrated intensity of the magnetic peak in (b) normalized to the (1 1 8) charge reflection.

FIG. 2. (Color online) (a) $[\zeta\ \zeta\ 0]$ scan through the magnetic Bragg peak position of the stripelike AFM phase at above (55 K) and below (20 K) T_N for the Ba(Fe$_{0.953}$Co$_{0.047}$)$_2$As$_2$ sample. The solid bar represents the experimental resolution for the x-ray measurements along this direction while the dashed bar denotes the resolution of our previous neutron measurements along this direction (Ref. 22). (b) $[\zeta\ -\zeta\ 0]$ scan through the magnetic Bragg peak position below T_N. The solid bar represents the experimental resolution along this direction for our x-ray measurements. The resolution width for neutron measurements (Ref. 22) along $[\zeta\ -\zeta\ 0]$ is a factor of ten larger. (c) and (d) correspond to (a) and (b), respectively, at the base temperature of 4.5 K. The difference in the vertical scale between panels (a), (b) and (c), (d) arises from small differences in the beam conditions for measurements performed several months apart.

early polarized perpendicular to the vertical scattering plane (σ polarized) with a spatial cross section of 1.0 mm (horizontal) $\times$ 0.2 mm (vertical). In this configuration, dipole resonant magnetic scattering rotates the plane of linear polarization into the scattering plane (π polarization). Cu(2 2 0) was used as a polarization analyzer to suppress the charge and fluorescence background relative to the magnetic scattering signal. For measurements of the magnetic reflections, the sample was mounted at the end of the cold finger of a displex cryogenic refrigerator with the tetragonal (*HHL*) plane coincident with the scattering plane.

In Figs. 1(a) and 1(b) we display the raw data for the parent BaFe$_2$As$_2$ compound for $[\xi\ \xi\ 0]$-scans through the (1 1 8)$_T$ charge peak and ($\frac{1}{2}$ $\frac{1}{2}$ 7)$_T$ magnetic peak positions above and below the coupled structural/magnetic transitions (T_S=$T_N$$\approx$136 K). These data were taken at the maximum in the resonant scattering (E=7.112 keV) at the Fe K edge. For temperatures below T_S (=T_N), the charge peak splits into the (2 0 8)$_O$ and (0 2 8)$_O$ peaks of the orthorhombic phase. The disparity in intensities is attributed to an imbalance in the domain populations for these reflections within the illuminated volume of the sample. Figure 1(b) shows that, below T_N, scattering is clearly observed at the (1 0 7)$_O$ magnetic
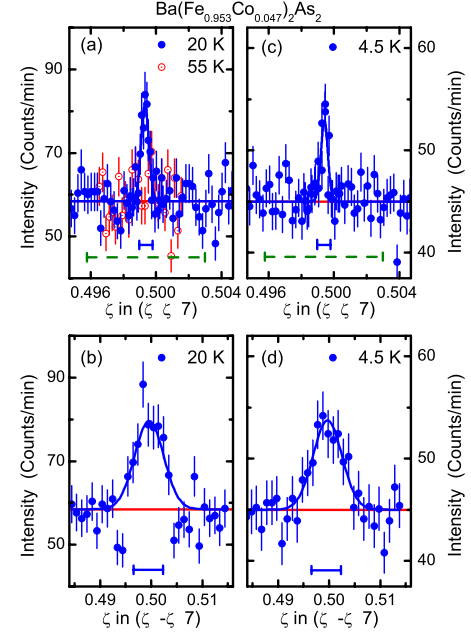
peak position in the orthorhombic phase with a_O>b_O. This diffraction peak arises from magnetic domains characterized by the propagation vector (1 0 1)$_O$ or ($\frac{1}{2}$ $\frac{1}{2}$ 1)$_T$. Magnetic scattering from domains characterized by the propagation vector (0 1 1)$_O$ or ($\frac{1}{2}$ $-\frac{1}{2}$ 1)$_T$ do not contribute to the scattering in this geometry. For simplicity, we will henceforth label all peaks with tetragonal indices. Therefore, (1 0 7)$_O$ will be referred to as ($\frac{1}{2}$ $\frac{1}{2}$ 7)$_T$, keeping in mind that the magnetic peaks are displaced from ζ=$\frac{1}{2}$ because of the orthorhombic distortion. The measured FWHM of 0.0007(1) rlu for the magnetic peak is the same (within error) as that of the charge peak, consistent with long-range magnetic order. Figure 1(c) shows that as the sample temperature increases, the intensity of the magnetic peak decreases until it can no longer be observed above background at approximately 140 K, in agreement with previous neutron-scattering measurements.[32]

For the Ba(Fe$_{0.953}$Co$_{0.047}$)$_2$As$_2$ sample, Fig. 2 shows scans along the $[\zeta\ \zeta\ 0]$ and transverse $[\zeta\ -\zeta\ 0]$ directions through the ($\frac{1}{2}$ $\frac{1}{2}$ 7)$_T$ magnetic Bragg peak position. For the $[\zeta\ \zeta\ 0]$ scan, the position of this peak is again referenced to the (1 1 8)$_T$ charge peak and is displaced from ζ=$\frac{1}{2}$ because

of the orthorhombic distortion [see Fig. 1(a)]. Along the $[\zeta \ \zeta \ 0]$ direction [Figs. 2(a) and 2(c)] and below T_N $=47$ K, we observe a single peak, whereas an incommensurability of magnitude ε would result in two peaks split by 2ε. The solid bar beneath the data in Figs. 2(a) and 2(c) describes the measured FWHM of the $(1\ 1\ 8)_T$ charge peak and represents our experimental resolution along $[\zeta \ \zeta \ 0]$. Therefore, the FWHM of 0.0007(1) rlu for the $(\frac{1}{2} \ \frac{1}{2} \ 7)_T$ magnetic Bragg peak along this direction places an upper limit on the potential incommensurability ($\varepsilon \approx 3.5 \times 10^{-4}$) which is two orders of magnitude smaller than the value proposed in Ref. 24. We have also checked along the transverse $[\zeta \ -\zeta \ 0]$ direction for any evidence of incommensurability as shown in Figs. 2(b) and 2(d). However, for the present experimental configuration, our resolution along this direction is coarser [0.0067(15) rlu]. Nevertheless, these data still allow us to place an upper limit on the incommensurability ($\varepsilon \approx 3.3 \times 10^{-3}$) that is more than an order of magnitude smaller than that proposed.[24] Furthermore, a comparison of the scans at 20 and 4.5 K shows that there is no evidence of additional line broadening for this compound below the superconducting transition ($T_c = 17$ K).

The dashed bars in Figs. 2(a) and 2(c) represent the experimental resolution for our previous neutron-diffraction measurements on Ba(Fe$_{0.953}$Co$_{0.047}$)$_2$As$_2$ along the $[\zeta \ \zeta \ 0]$ direction.[22] Even with the poorer resolution of this measurement, an incommensurability of $\varepsilon = 0.04$ rlu would have been clearly observed in scans performed along the $[\zeta \ \zeta \ 0]$ direction. Our XRMS measurements, however, now place a strong limit on the magnitude of any incommensurability for the Co-doped compound. In this light, the broadened line shapes measured by μSR,[25] NMR,[24] and Mössbauer spectroscopy[26] must arise from other causes. Density-functional-theory calculations by Kemper et al.[33] indicate that although the nonmagnetic scattering potential associated with Co doping in the FeAs planes is relatively well localized, the magnetic potential significantly perturbs the spin-density-wave state over much longer length scales. This, in turn, leads to a large distribution of hyperfine fields, as pointed out by Dioguardi et al.,[34] who suggest that the origin of the broadening in their NMR studies of Co- and Ni-doped BaFe$_2$As$_2$ is consistent with doping-induced disorder in the AFM state rather than incommensurate order.

We now turn to a description of the energy spectrum associated with the resonant scattering from BaFe$_2$As$_2$. In Fig. 3(a) we show the raw data from energy scans at constant $\mathbf{Q} = (\frac{1}{2} \ \frac{1}{2} \ 7)_T$ at $T = 6$ K (filled circles), well below T_N. To determine the background at this scattering vector, energy scans were also performed at $(\frac{1}{2} \ \frac{1}{2} \ 7)_T$ for $T = 140$ K (red triangles), just above T_N, and at $\mathbf{Q} = (0.45 \ 0.45 \ 7)$, away from the magnetic peak, at $T = 6$ K (open squares). The shape of the background in the vicinity of the Fe K edge is consistent with an increase in the fluorescence from the sample [Fig. 3(b)]. The background subtracted and absorption corrected energy scan at $(\frac{1}{2} \ \frac{1}{2} \ 7)_T$ shown in Fig. 3(c) contains several components: (1) an energy-independent contribution that is most clearly visible below the absorption edge; (2) a noticeable dip in the scattering intensity followed by; and (3) a sharp feature close to the absorption threshold
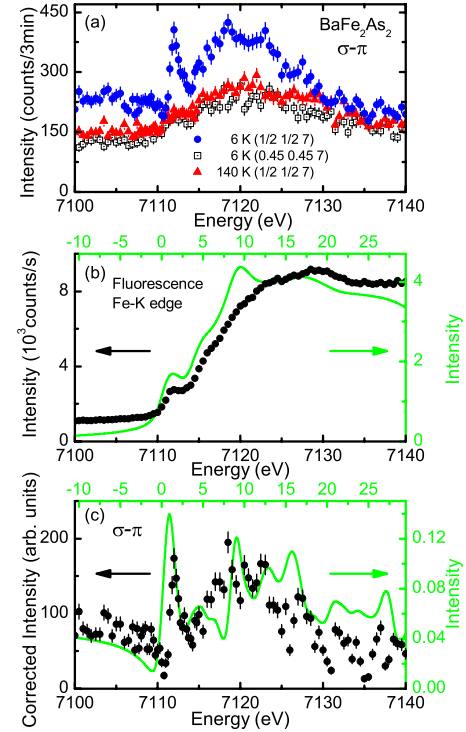

FIG. 3. (Color online) (a) Energy scans through the $(\frac{1}{2} \ \frac{1}{2} \ 7)_T$ magnetic peak above (filled triangles) and below (filled circles) T_N, and at low temperature away from the magnetic Bragg peak (open squares) (b) The measured fluorescence (filled circles) and calculated absorption (line) as described in the text. (c) The background subtracted and absorption corrected XRMS signal (filled circles) along with the calculated XRMS spectrum (line).

and broad scattering that extends to energies more than 20 eV above the absorption edge. This energy spectrum is similar to the one observed in previous XRMS measurements in the σ-π scattering channel at the Ni K edge for NiO.[35] The energy-independent scattering contribution (1) arises from nonresonant magnetic scattering while the resonant features (3) at and above the Fe K edge can be attributed to dipole ($E1$) transitions from the $1s$ initial state to the unoccupied $4p$ states that are weakly polarized through hybridization with $3d$ states near the Fermi energy. The sharp feature close to the absorption threshold may also contain a contribution from quadrupole ($E2$) allowed transitions from the $1s$ to $3d$ states but a clear separation of the $E1$ and $E2$ contributions will require further measurements of the angular dependence of the scattering as well as the σ-σ scattering channel. The dip in the scattering (2) arises from interference between the nonresonant and resonant magnetic scattering as the phase of the resonant scattering changes across the absorption edge.

To model the resonant scattering energy scans, we have used a FLAPW method[28] with a local density functional.[29] Details of the calculations will be presented elsewhere and only briefly outlined here. To obtain a self-consistent charge and potential, we chose 810 $\mathbf{k}$ points in the irreducible Brillouin zone (IBZ), and set $\mathbf{R}_{MT} \times \mathbf{k}_{max} = 8.0$, where R_{MT} is the smallest muffin-tin radius and k_{max} is the basis set cutoff (the maximum value of $|\mathbf{k} + \mathbf{K}_i|$ included in the basis). The

muffin-tin radii are 2.4 a.u., 2.2 a.u., and 2.2 a.u. for Ba, Fe, and As respectively. The self-consistent calculation was iterated until the total energy convergence reached 0.01 mRy/cell. For the x-ray absorption spectra [Fig. 3(b)] and XMRS [Fig. 3(c)] we calculated empty states up to 40 eV above Fermi energy with 1320 **k** points in IBZ and with the calculated self-consistent potential. Our calculation of the $E2$ contribution to the sharp feature close to the absorption threshold indicates that it is much smaller than the $E1$ contribution. To model the interference between the resonant and nonresonant scattering close to the absorption edge, an energy-independent scattering amplitude, equal to the resonant scattering contribution was added to the real part of the resonant scattering amplitude. The calculated energy spectrum was broadened with a 1.25 eV Lorentzian[36] to account for the core-hole lifetime, and a 1 eV Gaussian for the instrumental resolution. The calculated absorption and resonant scattering spectra are displayed as lines in Figs. 3(b) and 3(c), respectively, and capture the essential features of our measurements including features (1)–(3) discussed above.

In summary, we have used XRMS at the Fe K edge to directly probe the commensurability of the magnetic structure in Ba(Fe$_{0.953}$Co$_{0.047}$)$_2$As$_2$ with high resolution. The AFM structure is commensurate and the FWHM of scans measured along the [ζ ζ 0] direction places an upper limit on the potential incommensurability which is two orders of magnitude smaller than the value proposed in Ref. 24. Energy scans through the resonance at the Fe K edge are in reasonable agreement with theoretical calculations and these calculations suggest that the resonant scattering at the Fe K edge in the σ-to-π scattering channel arises from dipole allowed transitions from the core $1s$ states to the unoccupied $4p$ states that are spin polarized due to hybridization with the $3d$ states close to the Fermi energy.

[1] I. I. Mazin, D. J. Singh, M. D. Johannes, and M. H. Du, Phys. Rev. Lett. **101**, 057003 (2008).

[2] K. Kuroki, S. Onari, R. Arita, H. Usui, Y. Tanaka, H. Kontani, and H. Aoki, Phys. Rev. Lett. **101**, 087004 (2008).

[3] A. V. Chubukov, D. V. Efremov, and I. Eremin, Phys. Rev. B **78**, 134512 (2008).

[4] R. M. Fernandes *et al.*, Phys. Rev. B **81**, 140501 (2010).

[5] R. M. Fernandes and J. Schmalian, Phys. Rev. B **82**, 014521 (2010).

[6] A. B. Vorontsov, M. G. Vavilov, and A. V. Chubukov, Phys. Rev. B **79**, 060508(R) (2009).

[7] V. Cvetkovic and Z. Tesanovic, Phys. Rev. B **80**, 024512 (2009).

[8] T. M. Rice, Phys. Rev. B **2**, 3619 (1970).

[9] N. Lee and H. Choi, Phys. Rev. B **82**, 174508 (2010).

[10] A. B. Vorontsov, M. G. Vavilov, and A. V. Chubukov, Phys. Rev. B **81**, 174538 (2010).

[11] J. Park, D. Inosov, C. Yaresko, S. Graser, D. Sun, P. Bourges, Y. Sidis, Y. Li, J. Kim, D. Haug, A. Ivanov, K. Hradil, A. Schneidewind, P. Link, E. Faulhaber, I. Glavatskyy, C. Lin, B. Keimer, and V. Hinkov, Phys. Rev. B **82**, 134503 (2010).

[12] H.-F. Li *et al.*, Phys. Rev. B **82**, 140503 (2010).

[13] J. W. Lynn and P. C. Dai, Physica C **469**, 469 (2009).

[14] M. D. Lumsden and A. D. Christianson, J. Phys.: Condens. Matter **22**, 203203 (2010).

[15] C. de la Cruz *et al.*, Nature (London) **453**, 899 (2008).

[16] J. Zhao *et al.*, Nature Mater. **7**, 953 (2008).

[17] Q. Huang, J. Zhao, J. W. Lynn, G. F. Chen, J. L. Luo, N. L. Wang, and P. Dai, Phys. Rev. B **78**, 054529 (2008).

[18] Y. Chen, J. W. Lynn, J. Li, G. Li, G. F. Chen, J. L. Luo, N. L. Wang, P. Dai, C. dela Cruz, and H. A. Mook, Phys. Rev. B **78**, 064515 (2008).

[19] J. Zhao *et al.*, Phys. Rev. B **78**, 132504 (2008).

[20] D. H. Ryan, J. M. Cadogan, C. Ritter, F. Canepa, A. Palenzona, and M. Putti, Phys. Rev. B **80**, 220503 (2009).

[21] C. Lester, J.-H. Chu, J. G. Analytis, S. C. Capelli, A. S. Erickson, C. L. Condron, M. F. Toney, I. R. Fisher, and S. M. Hayden, Phys. Rev. B **79**, 144523 (2009).

[22] D. K. Pratt, W. Tian, A. Kreyssig, J. L. Zarestky, S. Nandi, N. Ni, S. L. Bud'ko, P. C. Canfield, A. I. Goldman, and R. J. McQueeney, Phys. Rev. Lett. **103**, 087001 (2009).

[23] A. Kreyssig *et al.*, Phys. Rev. B **81**, 134512 (2010).

[24] Y. Laplace, J. Bobroff, F. Rullier-Albenque, D. Colson, and A. Forget, Phys. Rev. B **80**, 140501 (2009).

[25] J. P. Carlo *et al.*, Phys. Rev. Lett. **102**, 087001 (2009).

[26] P. Bonville, F. Rullier-Albenque, D. Colson, and A. Forget, EPL **89**, 67008 (2010).

[27] F. L. Ning, K. Ahilan, T. Imai, A. S. Sefat, R. Jin, M. A. McGuire, B. C. Sales, and D. Mandrus, Phys. Rev. B **79**, 140506 (2009).

[28] P. Blaha, K. Schwarz, G. K. H. Madsen, D. Kvasnicka, and J. Luitz, Wien2K: An Augmented Plane Wave + Local Orbitals Program for Calculating Crystal Properties, (Karlheinz Schwarz, Techn. Universitat Wien, Austria 2001).

[29] J. P. Perdew and Y. Wang, Phys. Rev. B **45**, 13244 (1992).

[30] N. Ni, M. E. Tillman, J.-Q. Yan, A. Kracher, S. T. Hannahs, S. L. Bud'ko, and P. C. Canfield, Phys. Rev. B **78**, 214515 (2008).

[31] S. Nandi *et al.*, Phys. Rev. Lett. **104**, 057006 (2010).

[32] Q. Huang, Y. Qiu, W. Bao, M. A. Green, J. W. Lynn, Y. C. Gasparovic, T. Wu, G. Wu, and X. H. Chen, Phys. Rev. Lett. **101**, 257003 (2008).

[33] A. F. Kemper, C. Cao, P. J. Hirschfeld, and H.-P. Cheng, Phys. Rev. B **80**, 104511 (2009).

[34] A. Dioguardi, N. Roberts-Warren, A. Shockley, S. Bud'ko, N. Ni, P. Canfield, and N. Curro, Phys. Rev. B **82**, 140411(R) (2010).

[35] W. Neubeck, C. Vettier, F. de Bergevin, F. Yakhou, D. Mannix, O. Bengone, M. Alouani, and A. Barbier, Phys. Rev. B **63**, 134430 (2001).

[36] M. O. Krause and J. H. Oliver, J. Phys. Chem. Ref. Data **8**, 329 (1979).